Energy Efficient Parallel Concatenated Index Modulation and M-ary PSK Aided OFDM-DCSK Communications With QoS Consideration

Zhaofeng Liu, Lin Zhang, *Senior Member, IEEE*, Zhiqiang Wu, *Senior Member, IEEE*, and Yuan Jiang

***Abstract*—In this paper, we propose a parallel concatenated index modulation and M-ary phase shift keying (MPSK) to integrate with carrier interferometry (CI) codes into the orthogonal frequency division multiplex (OFDM) differential chaotic shift keying (DCSK) communication system. Our objective is to meet different quality of service (QoS) user demands while achieving higher energy efficiency and retaining reliable communications with low peak-to-average power ratio (PAPR). In our design, one input bit set is modulated by the index of the CI codes matrix whose rows are rotated circularly, another bit set is mapped to the MPSK symbols to realize the M-ary modulation. Subsequently, the resultant MPSK symbols are modulated by reference chaotic sequences and spread by the information-bearing rotated CI codes matrix at the transmitter. After the OFDM modulations, the information bearing symbols are transmitted over multiple subcarriers. At the receiver, after the non-coherent chaotic correlation demodulation, the maximum likelihood detection method is firstly applied to attain the estimates of the index modulated bit set, which are then used to recover the phases of chaotic sequences for further evaluation of another MPSK modulated symbols. Since no additional energy is required while more bits can be transmitted via the M-ary modulation and index modulation, the energy efficiency can be improved. In addition, thanks to the orthogonality of the CI codes matrix and the spreading in the frequency domain, the PAPR could be suppressed and reliability performances can be improved. Then theoretical analysis is conducted and simulation results validate the theoretical analysis. Moreover, the results demonstrate the superior bit error rate (BER) performances to benchmarks and flexible data rate could be provided for user terminals via different combinations of the index modulation and the M-ary modulation.**

***Index Terms*—Carrier interferometry spreading, energy efficiency and quality of service (QoS), index modulation, orthogonal frequency division multiplex-based differential chaos shift keying (OFDM-DCSK), parallel concatenated high order modulation.**

Manuscript received January 26, 2020; revised May 16, 2020; accepted June 8, 2020. Date of publication June 15, 2020; date of current version October 13, 2020. This work was supported in part by the Guangdong Basic and Applied Basic Research Foundation under Grant 2020A1515010703, in part by the Open Research Fund from Shandong Provincial Key Laboratory of Wireless Communication Technologies under Grant SDKLWCT-2019-05, in part by Key Research and Development and Transformation Plan of Science and Technology Program for Tibet Autonomous Region under Grant XZ201901-GB-16, in part by the Special Fund from the Central Finance to Support the Development of Local Universities under Grant ZFYJY201902001, in part by the National Science Foundation of China under Grant 61602531, in part by National Science Foundation under Grant 1748494, and in part by OFRN. The review of this article was coordinated by Prof. S.-H. Leung. *(Corresponding author: Lin Zhang.)*

Zhaofeng Liu is with the School of Electronics and Information Technology, Sun Yat-sen University, Guangzhou 510006, China (e-mail: liuzhf5@mail2.sysu.edu.cn).

Lin Zhang is with the School of Electronics and Information Technology, Sun Yat-sen University, Guangzhou 510006, China, and also with the Shandong Provincial Key Laboratory of Wireless Communication Technologies, Jinan 250100, China (e-mail: isszl@mail.sysu.edu.cn).

Zhiqiang Wu is with the Department of Electrical Engineering, Tibet University, Lhasa 850000, China, and also with the Wright State University, Dayton, OH 45435 USA (e-mail: zhiqiang.wu@wright.edu).

Yuan Jiang is with the Nanhai Research Institute, Sun Yat-sen University, Guangzhou 510275, China (e-mail: jiangyuan3@mail.sysu.edu.cn).

Digital Object Identifier 10.1109/TVT.2020.3002067

I. Introduction

CHAOTIC communications have attracted a lot of research interests thanks to their anti-multi-path-fading capabilities. They have been widely used in wireless systems to provide transmission services for users ends such as Internet of Things (IoT) terminals or machines etc. Each user equipment has different quality of service (QoS) demands [1]. For example, due to limited battery capacity, IoT user equipment wants to transmit information with high energy efficiency, while machine to machine (M2M) communications [2] requires high-reliability performances.

The chaos-based modulation schemes [3]–[5] have two main types, which are coherent chaos shift keying (CSK) [5] and non-coherent differential chaos shift keying (DCSK) [6] based schemes. Since the chaos synchronization circuit at CSK receivers has high complexity and is difficult to implement, DCSK [6] is regarded as a more practical scheme and has attracted more research interests.

However, the conventional DCSK has the energy efficiency as low as $1/2$ since half of the time slots are used to deliver chaotic reference sequences [7]–[11]. Many research works have been conducted to improve the energy efficiency of single carrier DCSK systems. Researchers propose a quadrature chaos shift keying [7] (QCSK) and a high-efficiency DCSK [8] (HE-DCSK) schemes to improve the energy efficiency by carrying more bits on the chaotic sequences orthogonal to the chaotic reference sequences via the Hilbert transformation. Moreover, the Walsh code spread DCSK systems [12], [13] use Walsh codes to carry more bits, while M-ary DCSK systems [14], [15] apply M-ary modulation to improve the energy efficiency.

Recently, the index modulation (IM), which uses index bits to modulate some indexes such as the time index, the subcarrier index and the spacial modulation order index [16]–[18], has been proposed to improve the energy efficiency by transmitting more bits with no additional symbol energy required. Then researchers apply the IM to DCSK systems [19]–[21] to utilize the index

of Walsh codes to improve energy efficiency by delivering index bits without the usage of extra symbols. Besides, [22] and [23] use index bits to control the order of chaotic sequences, while [24] uses index bits to transmit the carrier index. Thus with the aid of the index modulation, the energy efficiency could be effectively enhanced.

To further improve the energy efficiency and address another issue of the DCSK scheme [6] that the delay line circuit is difficult to be implemented in practical systems [25], multi-carrier (MC) based transmission schemes such as MC-DCSK [9] and orthogonal frequency division multiplexing (OFDM) DCSK [10], [11] have been proposed. In MC based DCSK schemes [21], one subcarrier is used to transmit chaotic reference sequences, and other subcarriers are used to transmit information-bearing chaotic sequences, which means that $N-1$ information-bearing chaotic sequences will share one chaotic reference sequence where N is the number of subcarriers. Therefore, the energy efficiency can be improved, especially for large N in the new radio system. Moreover, the direct transmission of the chaotic reference signal removes the delay line circuits, thus the system complexity is significantly dropped and the practicality of implementing the system is enhanced.

Although both single carrier M-ary DCSK modulations and MC-DCSK schemes improve the energy efficiency, overlapping operations implemented in these schemes bring the problem of a high peak-to-average power ratio (PAPR). In [26], the authors proposed a low PAPR MC-M-ary DCSK scheme. Then in our previous work [27], we propose to utilize the carrier interferometry (CI) codes to spread the symbols in the frequency domain to suppress the PAPR. Different from binary spreading codes like Walsh code, CI code is a kind of phase code, which can enable the subcarriers to be added non-coherently, thus the PAPR performance of CI codes spreading multi-carrier system could be improved.

Till now, few research works have been done to simultaneously improve energy efficiency and suppress the PAPR with the considerations of different QoS demands. Notably, QoS usually corresponds to a set of predefined service performance [28]. In this paper, we mainly focus on the service performances of the data rate and the reliability of information transmissions in the physical layer. In order to achieve higher energy efficiency, lower PAPR, and adaptable BER performances to meet different QoS demands, we propose a parallel concatenated index modulation and M-ary phase-shift keying (MPSK) modulation (PC-IM-MPSK) scheme to integrate with CI codes into the OFDM-DCSK system.

Different from our previous research work presented in [27], [29], and existing research achievements, we utilize the index of the CI codes matrix to deliver the information bits. Then we take QoS demands into account and propose a parallel concatenated index modulation and MPSK scheme to integrate into OFDM-DCSK systems. Furthermore, we analyze the theoretical BER performances, energy efficiency, spectral efficiency, complexity, and security performances.

In our design of the parallel concatenated index modulation and MPSK aided OFDM-DCSK (PC-IM-MPSK-OFDM-DSCK) scheme, the input data bits are divided into two parallel subsets. One bit set is modulated by the index of the CI codes matrix, while another set is modulated by the MPSK modulation module. The first set of bits is converted to the decimal number as the index for further circular rotation of the rows of the CI codes matrix. Meanwhile, the bits in another set are mapped to MPSK symbols. Subsequently, the MPSK symbols are modulated by the chaotic sequence. Since chaotic chips are noise-like and aperiodic, the amplitudes of information-bearing symbols would be modulated by chaotic chips and also become chaotic. Therefore, in order to avoid the interference to the amplitude variant chaotic signals, we would not use the quadrature amplitude modulation (QAM) scheme to modulate the information bit set. Instead, we apply the MPSK modulation and the resultant MPSK symbols will have constant envelops. Thus the interference can be mitigated.

Then the resultant chaotic modulated symbols are spread by the information-bearing CI codes matrix. After performing the inverse fast Fourier transform (IFFT) and adding the cyclic prefix (CP), the OFDM-DCSK symbols are transmitted via channels. At the receiver, after removing the CP and performing the fast Fourier transform (FFT), the maximum likelihood (ML) detection is carried out to demodulate the index modulated bits. Then the CI codes matrix is obtained to be used for the chaotic demodulation. Thus after the MPSK demodulation, the estimates of another bit set can also be obtained.

Since the proposed transmitter can carry more bits thanks to the M-ary modulation and index modulation without introducing additional chaotic reference sequence, both the energy efficiency and the spectral efficiency can be improved. Moreover, the parallel concatenation architecture makes it possible to flexibly adjust the data rate and the bit error rate (BER) to meet different QoS demands of users. Furthermore, the spreading achieved by the CI codes matrix can suppress the PAPR.

Briefly, the main contributions of this paper include:

1) We propose the parallel concatenation architecture of the index modulation and MPSK scheme; thus the equivalent modulation order can be flexibly adjusted to meet different QoS demands of the data rate and BER of multiple users.
2) We propose to utilize the index of the CI codes matrix to deliver information bits; thus more bits can be delivered with no need for additional energy, and the energy efficiency can be improved. Moreover, by spreading the chaotic modulated symbols by the information-bearing CI codes matrix, the PAPR can also be suppressed.
3) We derive the theoretical BER expressions and provide energy efficiency, spectral efficiency. PAPR and complexity performances analysis of our proposed design. Simulation results verify the effectiveness of our derivations and demonstrate that our design outperforms counterpart schemes.

This paper is organized as follows. Section II describes in detail the proposed PC-IM-MPSK-OFDM-DSCK system, including the transmitter and the receiver structures. Then in Section III, we provide the theoretical analysis including the spectral efficiency, energy efficiency, PAPR, BER and computational complexity. Subsequently, Section IV presents the simulation results for comparisons with the theoretical analysis

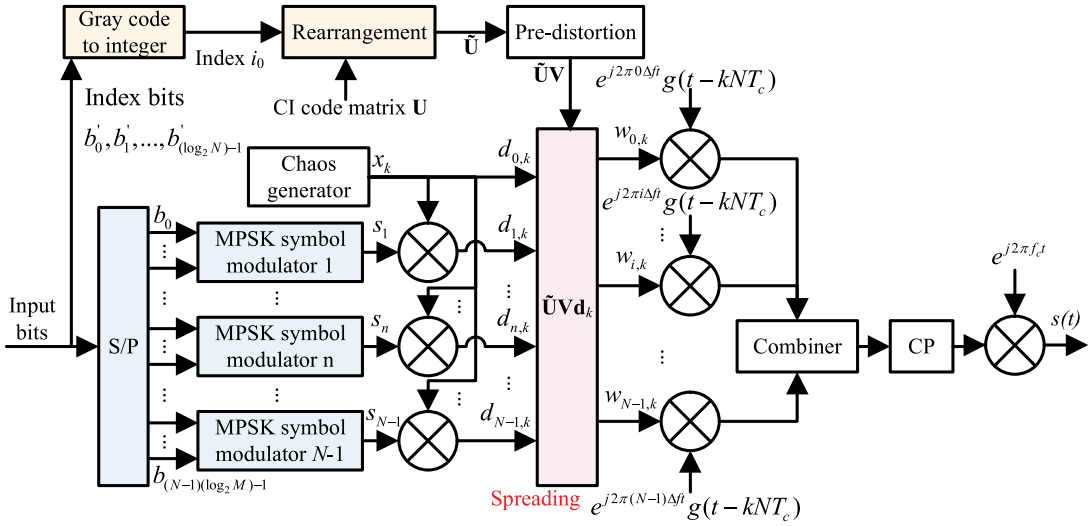

Fig. 1. Transmitter structure.

and the benchmark schemes. Finally, Section V concludes our findings.

II. Parallel Concatenated Index Modulation and MPSK Aided OFDM-DCSK Design

In this section, we present the transceiver structure of the PC-IM-MPSK-OFDM-DCSK in detail.

A. Transmitter Structure

Figure 1 illustrates the transmitter structure using the PC-IM-MPSK-OFDM-DSCK scheme. The input information bits are divided into two sets. The first set of bits is converted to the decimal number based on which the row of the CI codes matrix is circularly rotated. Meanwhile, another set of bits are modulated by the MPSK module. It is worth pointing out that since different bit rate and different BER could be provided by the CI code index modulation and the MPSK scheme, the division of input bits would be based on the QoS demands of the user data to be delivered. In addition, in the following discussions, without loss of generality, the available subcarriers are also assumed to be occupied by a single user [21], [24], while different services from the user could be delivered in our proposed system. Thus no multi user interference would be considered in the performance analysis.

Subsequently, the MPSK symbols are modulated by the chaotic reference sequence. Then the chaotic modulated symbols are spread by the information-bearing CI codes matrix in the frequency domain to suppress the PAPR. After IFFT and adding CP, the OFDM symbols are transmitted over multiple subcarriers. More details are given as follows.

1) Index Modulation: The CI codes matrix can provide the phase offset for the OFDM symbol over different subcarriers. With the help of the phase offset brought by CI codes, the signals delivered via multiple subcarriers can be added non-coherently, thus the envelop of the overall OFDM waveform fluctuates slightly. As a result, the PAPR can be reduced. One CI code is denoted as $u_i^{(n)} = e^{j2\pi \cdot i \cdot n/N}$ [27], which represents the phase offset on the nth symbol over the ith subcarrier. Notably, the CI codes matrix is a square matrix and has a dimension of $N \times N$. Thus the elements $u_i^{(n)}(i = 0, 1, \ldots, N-1)$ constitute a column vector $\mathbf{u}_n = [u_0^{(n)}, u_1^{(n)}, \ldots, u_i^{(n)}, \ldots, u_{N-1}^{(n)}]^T$. The length of $\mathbf{u}_n$ should be N. It is noticeable that these column vectors are orthogonal to each other, i.e., $\mathbf{u}_{n_1}^T \mathbf{u}_{n_2} = \sum_{i=0}^{N} e^{j2\pi \cdot i \cdot (n_1+n_2)/N} = 0$ when $n_1 \neq n_2$. Then all column vectors constitute the CI codes matrix, which is denoted as $\mathbf{U} = [\mathbf{u}_0, \mathbf{u}_1, \ldots, \mathbf{u}_n, \ldots, \mathbf{u}_{N-1}]$.

In the index modulation, the maximum number of bits that the CI codes matrix can carry is $N_i = \log_2 N$. Thus the first set of bits is represented by $b_0', b_1', \ldots, b_{(\log_2 N)-1}'$ which are converted to a decimal number denoted by i_0. Then i_0 having the range of $0 \leq i_0 \leq N-1$ is used to rotate the row of the CI codes matrix circularly $\mathbf{U}$. It is worth pointing out that the orthogonality between the column vectors of the CI codes matrix helps to the reliable information retrieval at the receiver.

After the circular rotation with i_0, we obtain the information-bearing rotated matrix $\tilde{\mathbf{U}}$ as:

$$\tilde{\mathbf{U}} = [\tilde{\mathbf{u}}_0, \tilde{\mathbf{u}}_1, \ldots, \tilde{\mathbf{u}}_n, \ldots, \tilde{\mathbf{u}}_{N-1}], \tag{1a}$$

$$\tilde{\mathbf{u}}_n = [u_{i_0}^{(n)}, u_{i_0+1}^{(n)}, \ldots, u_{i_0+i}^{(n)}, \ldots, u_{i_0+N-1}^{(n)}]^T, \tag{1b}$$

$$u_{i_0+i}^{(n)} = e^{j2\pi \cdot (i_0+i) \cdot n/N}. \tag{1c}$$

It can be observed from (1a) to (1c) that the order of the column vectors in $\tilde{\mathbf{U}}$ are circularly rotated.

2) M-Ary DCSK Modulation: The information bits of another set are mapped as MPSK constellation symbols. Then they are modulated by the chaotic reference sequence output from the chaos generator. More explicitly, at the chaos generator, the chaotic sequence is generated with the second-order Chebyshev polynomial function (CPF) $x_{k+1} = 1 - 2x_k^2, k = 0, 1, \ldots, \beta - 1$, where β denotes the length, $x_k \in (-1, 0) \cup (0, 1)$ is the kth

chip and the initial value x_0 is a predefined value shared between transceivers.

Then the chaotic sequence is used to modulate the MPSK symbol. The chaotic sequence has the property of being aperiodic, noise-like and sensitive to the initial value, thus the information could be hidden behind the irregular chaotic behaviors, thus the security of transmissions could be enhanced. Considering that the chaotic sequence would be transmitted together with the chaotic modulated symbols, to facilitate the expression, let $s_0 = 1$, and $s_n, n > 0$ denote the nth MPSK symbol. The symbols input to the IFFT module are represented by:

$$d_{n,k} = s_n x_k. \tag{2}$$

Then we denote the kth chip to be modulated by the OFDM module in the form of a vector which is represented by $\mathbf{d}_k = [d_{0,k}, d_{1,k}, \ldots, d_{n,k}, \cdots, d_{N-1,k}]^T$, where $(\cdot)^T$ represents the transposition operation.

Obviously, the number of information bits modulated by the MPSK might be different from that by the index modulations presented above. Thus the parallel index modulation and the MPSK modulation will enable the proposed system to provided different bit rate for user data collected from different users. Hence different QoS in terms of the data rate could be provided.

3) Pre-Distortion and CI Coded Spreading: After the parallel index modulation and MPSK modulation, the MPSK symbols $\mathbf{d}_k$ will be spread by the information-bearing rotated CI codes matrix $\tilde{\mathbf{U}}$, as marked with red color in Fig. 1. Considering that the information bits carried by $\tilde{\mathbf{U}}$ will induce the phase offset when performing de-spreading operations at the receiver, we propose to add a pre-distortion module at the transmitter to combat the phase offset and to avoid the phase ambiguity which might induce high BER.

The pre-distortion operation is performed by using a diagonal matrix $\mathbf{V}$ represented by:

$$\mathbf{V} = \mathrm{diag}([V_{i_0,0}, V_{i_0,1}, \ldots, V_{i_0,n}, \ldots, V_{i_0,N-1}]), \tag{3}$$

where $\mathrm{diag}(\cdot)$ transforms a vector to a diagonal matrix, and $V_{i_0,n} = e^{-j2(M-1)\pi i_0 n/(MN)}$.

Thus after the pre-distortion, the rotated CI codes matrix becomes $\tilde{\mathbf{U}}\mathbf{V}$, whose vectors are denoted by $\tilde{\mathbf{u}}_n V_{i_0,n}$ and remain orthogonal with each other. Moreover, since the amplitude of $V_{i_0,n}$ in $\mathbf{V}$ is 1, the pre-distortion module will not increase the PAPR.

Next, the chaotic modulated M-ary symbols $\mathbf{d}_k$ are spread by the pre-distorted CI codes matrix $\tilde{\mathbf{U}}\mathbf{V}$ in the frequency domain as follows:

$$\mathbf{w}_k = \tilde{\mathbf{U}}\mathbf{V}\mathbf{d}_k = [w_{0,k}, w_{1,k}, \cdots, w_{i,k}, \ldots, w_{N-1,k}]^T, \tag{4}$$

where $w_{i,k}$ is the kth information-bearing chaotic modulated chip to be transmitted over the ith subcarrier.

4) OFDM Modulation: In the OFDM module, IFFT is performed on $\mathbf{w}_k$ restricted in the duration of a rectangular pulse shaping waveform $g(t - kNT_c)$, where T_c denotes the chip duration. Besides, the frequency interval of orthogonal subcarriers is Δf, which is small enough to ensure the orthogonality. After the IFFT, the resultant waveform $s(t)$ is expressed as:

$$\begin{aligned} s(t) &= \sum_{k=0}^{\beta-1}\sum_{i=0}^{N-1} w_{i,k} e^{j2\pi(f_c+i\Delta f)t} \times g(t - kNT_c - kT_{CP}) \\ &= \sum_{k=0}^{\beta-1}\sum_{n=0}^{N-1} d_{n,k} \sum_{i=0}^{N-1} e^{j\frac{2\pi}{N}\cdot(\frac{i_0}{M}+i)\cdot n} e^{j2\pi(f_c+i\Delta f)t} \\ &\quad \times g(t - kNT_c - kT_{CP}), \end{aligned} \tag{5}$$

where the time duration of $s(t)$ is $T_s = \beta T_{OFDM} = \beta N T_c$ and T_{OFDM} is the duration of an OFDM symbol [11]. Moreover, T_{CP} denotes the duration of CP, f_c denotes the center frequency of subcarriers, then the frequency interval is defined as $\Delta f = 1/T_{OFDM}$. Additionally, $g(t - kNT_c - kT_{CP})$ denotes the rectangular pulse shaping waveform for the kth chip with the time delay of $kNT_c + kT_{CP}$.

B. Receiver Structure

At the receiver, the signal received from the channel can be denoted in the time domain as:

$$r(t) = h(t) \otimes s(t) + n(t), \tag{6}$$

where $\otimes$ denotes the cyclic convolution operator, $n(t)$ denotes the complex Gaussian noise, which has mean value zero and power spectral density N_0, and $h(t)$ represents the overall channel response. For multi-path fading channel, $h(t) = \sum_{l=1}^{L} \alpha_l \delta(t - \tau_l)$ [11], where L denotes the number of paths, α_l and τ_l, respectively, denote the independent and identically distributed (i.i.d) fading coefficient and path delay, which remain constant during the overall OFDM-DCSK symbol duration T_s for the lth path and $\delta(\cdot)$ denotes the unit impulse function.

As shown in Fig. 2, after the down-conversion transformation and the removal of CP, the OFDM demodulation and inverse CI de-spreading are performed. Then, chaotic demodulation is carried out with the chaotic reference sequence. The resultant symbols are then demodulated sequentially to provide the estimates of two information sets for user equipment. More details are presented as follows.

1) OFDM Demodulation: As shown in Fig. 2, the received signal will be replicated N times, and the resultant N data streams will be demodulated with the orthogonal waveform $e^{-j2\pi i\Delta f t} g(t - kNT_c)$. The obtained symbols in the kth received vector can be denoted as $\mathbf{r}_k = [r_{0,k}, \ldots, r_{i,k}, \ldots, r_{N-1,k}]^T$.

Under the assumption that the phase of the channel frequency response over the ith subcarrier can be estimated and counteracted with perfect channel estimation, while perfect channel state information (CSI) could be learned at the receiver [30], the received symbol $r_{i,k}$ can be calculated by:

$$r_{i,k} = H_{i,k} \sum_{m=0}^{N-1} d_{m,k} u^{(m)}_{\frac{i_0}{M}+i} + \xi_{i,k}, \tag{7}$$

where $\xi_{i,k}$ denotes the complex Gaussian noise with the mean value of 0 and the variance of N_0. $H_{i,k}$ denotes the channel frequency response for the kth chaotic chip over the ith subcarrier,

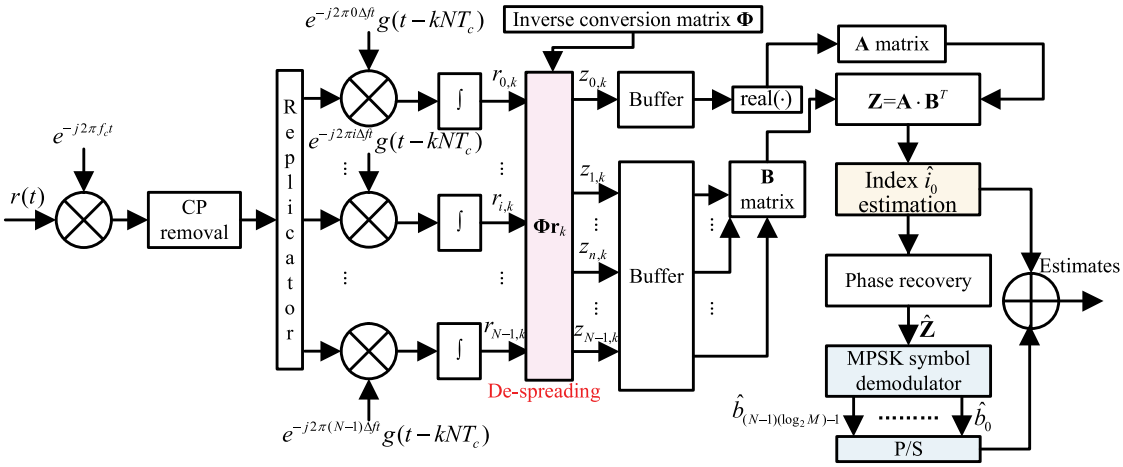

Fig. 2. Receiver structure.

which remains constant in the overall OFDM-DCSK symbol duration T_s. That is to say, for $\forall k^{'} \neq k$, in the duration of T_s, we have $H_{i,k} = H_{i,k'} = H_i$.

2) CI Codes De-Spreading: Subsequently, $\mathbf{r}_k$ is de-spread with the inverse CI codes matrix $\mathbf{\Phi}$ represented by $\mathbf{\Phi} = [\boldsymbol{\phi}_0, \boldsymbol{\phi}_1, \ldots, \boldsymbol{\phi}_n, \ldots, \boldsymbol{\phi}_{N-1}]^T$, where $\boldsymbol{\phi}_n = [\phi_0^{(n)}, \phi_1^{(n)}, \ldots, \phi_i^{(n)}, \ldots, \phi_{N-1}^{(n)}]^T$ and $\phi_i^{(n)} = e^{-j2\pi \cdot i \cdot n/N} = u_i^{(-n)}$.

As mentioned above, thanks to the orthogonality of $\tilde{\mathbf{u}}_n V_{i_0,n}$, we have $\tilde{\mathbf{u}}_n V_{i_0,n} \bullet \mathbf{v}_m = N e^{j\pi i_0 n}$ when $n = m$, $\bullet$ denotes the dot product between two vectors. and $\tilde{\mathbf{u}}_n V_{i_0,n} \bullet \mathbf{v}_m = 0$ when $n \neq m$.

Therefore, according to (7), the kth chip of the nth de-spread data $z_{n,k}$ can be denoted as:

$$\begin{aligned} z_{n,k} &= \boldsymbol{\phi}_n \bullet \mathbf{r}_k = \sum_{i=0}^{N-1} r_{i,k} \phi_i^{(n)} \\ &= \underbrace{\sum_{i=0}^{N-1} H_i x_k \left(\sum_{m=0}^{N-1} s_m u_{\frac{i_0}{M}}^m u_i^{(m-n)} \right)}_{A_{n,k}} + \underbrace{\sum_{i=0}^{N-1} \xi_{i,k}^{(n)}}_{B_{n,k}} \end{aligned} \tag{8}$$

where $A_{n,k}$ and $B_{n,k}$ denote the signal and noise term in $z_{n,k}$, respectively [29]. Notably, when $n = 0$, $z_{0,k}$ denotes the kth reference chaotic chip, while when $n \geq 1$, $z_{n,k}$ denotes the kth information-bearing chaotic chip. Besides, $\xi_{i,k}^{(n)} = \xi_{i,k} v_i^{(n)}$ and $\xi_{i,k}^{(n)}$ have the same mean value and variance as $\xi_{i,k}$.

Then the vector constituted by de-spread symbols is represented by:

$$\mathbf{z}_k = \mathbf{V}\mathbf{r}_k = [z_{0,k}, z_{1,k}, \ldots, z_{n,k}, \ldots, z_{N-1,k}]^T. \tag{9}$$

3) Correlation Chaotic Demodulation: Next, the obtained de-spread chaotic chips will be stored in the buffer and released for chaotic demodulation every β chaotic chips duration. Notably, considering that the chaotic chip used at the transmitter is real, hence we propose to only use the real part of the received reference chaotic chips for correlation demodulation.

Thus, the reference chaotic chips matrix $\mathbf{A}$ and the information-bearing chips matrix $\mathbf{B}$ are represented by:

$$\mathbf{A} = \begin{bmatrix} \mathbb{R}\{z_{0,0}\} & \mathbb{R}\{z_{0,1}\} & \cdots & \mathbb{R}\{z_{0,\beta-1}\} \end{bmatrix} \tag{10a}$$

$$\mathbf{B} = \begin{bmatrix} z_{1,0} & z_{1,1} & \cdots & z_{1,\beta-1} \\ z_{2,0} & z_{2,1} & \cdots & z_{2,\beta-1} \\ \vdots & \vdots & \ddots & \vdots \\ z_{N-1,0} & z_{N-1,1} & \cdots & z_{N-1,\beta-1} \end{bmatrix} \tag{10b}$$

where $\mathbb{R}\{\cdot\}$ takes the real part of a complex number, $z_{0,k}$ denotes the kth element of the demodulated chaotic reference sequence, $z_{n,k}$ $(n > 0)$ denotes the kth element of the demodulated information-bearing chaotic sequence.

Applying the chaotic correlation modulation on $\mathbf{A}$ and $\mathbf{B}$, we attain the information-bearing symbol matrix as:

$$\mathbf{Z} = \mathbf{A} \cdot \mathbf{B}^T = \begin{bmatrix} Z_1 & Z_2 & \cdots & Z_{N-1}, \end{bmatrix} \tag{11}$$

where $Z_n = \sum_{k=0}^{\beta-1} \mathbb{R}\{z_{0,k}\} \cdot z_{n,k}$.

4) Index Demodulation, Phase Recovery, and Data Symbol Estimation: Subsequently, the index demodulation, and the MPSK demodulation are carried out to recover the information.

Firstly, we evaluate i_0. Let $\hat{i}$ denote the estimate of index symbol. Corresponding to the pre-distortion module, we compensate the phase offset induced by i_0 to Z_n and obtain

$$Z_{n,\hat{i}} = Z_n e^{-j2\pi \hat{i} \cdot n/(MN)} = Z_n \phi_{\hat{i}/M}^{(n)}. \tag{12}$$

To be more specific, $Z_{n,\hat{i}}$ can be calculated by:

$$\begin{aligned} Z_{n,\hat{i}} = Z_n \phi_{\frac{\hat{i}}{M}}^{(n)} = \phi_{\frac{\hat{i}}{M}}^{(n)} \sum_{k=0}^{\beta-1} \big(& A_{0,k}^* A_{n,k} + A_{0,k}^* B_{n,k} \\ & + B_{0,k}^* A_{n,k} + B_{0,k}^* B_{n,k} \big), \end{aligned} \tag{13}$$

where the first term $A_{0,k}^* A_{n,k}$ represents the desired signal, while other terms represent interference. Moreover, $A_{n,k}$ can

be evaluated by:

$$A_{n,k} = x_k \sum_{i=0}^{N-1} H_i \left(\sum_{m=0}^{N-1} s_m u_{\frac{i_0}{M}}^{(m)} u_i^{(m-n)} \right)$$
$$= \underbrace{x_k s_n u_{\frac{i_0}{M}}^{(n)} N\overline{H}}_{C_{n,k}} + \underbrace{x_k \sum_{i=0}^{N-1} H_i \left(\sum_{m=0 m\neq n}^{N-1} s_m u_{\frac{i_0}{M}}^{(m)} u_i^{(m-n)} \right)}_{D_{n,k}} \tag{14}$$

where $C_{n,k}$ contains the kth chip of the desired nth symbol, $D_{n,k}$ denotes the inter-symbol interference and $\overline{H} = \sum_{i=0}^{N-1} H_i/N$.

Substituting (13) into (14), except the desired signal item $C_{n,k}$, we categorize all other items as the interference and noise denoted by $I_{0,n,k}$, then (13) is rewritten as:

$$Z_{n,\hat{i}} = \phi_{\frac{\hat{i}}{M}}^{(n)} \sum_{k=0}^{\beta-1} (C_{0,k}^* C_{n,k} + I_{0,n,k})$$
$$= \underbrace{s_n u_{\frac{i_0-\hat{i}}{M}}^{(n)} N^2 \overline{H}^2 \sum_{k=0}^{\beta-1} x_k^2}_{\text{desired signal}} + \underbrace{\sum_{k=0}^{\beta-1} \phi_{\frac{\hat{i}}{M}}^{(n)} I_{0,n,k}}_{\text{overall interference}} \tag{15}$$

Since $u_{(i_0-\hat{i})/M}^{(n)} = e^{j2\pi\cdot(i_0-\hat{i})\cdot n/(MN)}$, it could be seen from the above equation that the value of i_0 determines the argument of the desired signal.

Then we could utilize the argument of constellation points to evaluate i_0. We first find the MPSK constellation point which has the lowest Euclidean distance with $Z_{n,\hat{i}}$, which is denoted by $\zeta_{n,\hat{i}}$. Let $\eta_{n,\hat{i}}$ denote the argument of $Z_{n,\hat{i}}$, $\psi_{n,\hat{i}}$ denote the argument of $\zeta_{n,\hat{i}}$, then we can derive the optimal estimate of the row index i_0, which is denoted as $\hat{i}_0$, as follows:

$$\hat{i}_0 = \arg\min_{\hat{i}} \sum_{n=1}^{N-1} |\eta_{n,\hat{i}} - \psi_{n,\hat{i}}| \tag{16}$$

As shown in (16), by minimizing the phase offset between $Z_{n,\hat{i}}$ and $\zeta_{n,\hat{i}}$, the optimal $\hat{i}$ can be calculated as $\hat{i} = \hat{i}_0$, thus the estimate of i_0 can be obtained.

Moreover, from (15) and (16), we can find that the estimated $\hat{i}$ is closely related to $Z_{n,\hat{i}}$; therefore, the optimal phase of $Z_{n,\hat{i}}$ can be calculated using $\hat{i}_0$. Assuming that the overall interference can be ignored in the following analysis when $i_0 - \hat{i} \neq 0$, the phase of $Z_{n,\hat{i}}$ changes with different n, and the number of the phase can vary considerably compared with the phase $\psi_{n,\hat{i}}$ of the constellation points. Otherwise, when $i_0 - \hat{i} = 0$, the phase of $u_{i_0-\hat{i}}^{(n)}$ is equal to 0, then the phase value $\eta_{n,\hat{i}}$ of $Z_{n,\hat{i}}$ varies little with n and becomes equal to the phase value $\psi_{n,\hat{i}}$ of the constellation points $\zeta_{n,\hat{i}}$.

Accordingly, with the aid of $\hat{i}_0$, the phase recovery can be performed to attain the estimate of $\mathbf{Z}$ as:

$$\hat{Z}_n = Z_n \cdot e^{-\frac{j2\pi\hat{i}_0 n}{MN}} = e^{-\frac{j2\pi\hat{i}_0 n}{MN}} \sum_{k=0}^{\beta-1} \mathbb{R}\{z_{0,k}\} \cdot z_{n,k}, \tag{17}$$

where $\hat{Z}_n$ is the estimate of MPSK symbols. Notably, $\sum_{k=0}^{\beta-1} \mathbb{R}\{z_{0,k}\} \cdot z_{n,k}$ could be further denoted by $\rho e^{j2\pi i_0 n/(MN)}$, where ρ represents the part containing the desired symbol without the phase offset brought by CI codes spreading and the index modulation. We can see that if the estimated index symbol $\hat{i}_0$ deviates from the original transmitted index symbol i_0, the phase of the resultant symbol $\hat{Z}_n$ will be rotated, which leads to the BER performance degradation. Then after the parallel to serial (P/S) conversion, the transmitted information bits can be retrieved.

III. Performance Analysis

In this section, we present the energy efficiency, spectral efficiency, PAPR, BER, and complexity performances analysis for our proposed system.

A. Energy Efficiency and Spectral Efficiency

Without loss of generality, in the energy efficiency analysis, we ignore the energy cost of the CP.

Define E_{data} and E_{ref} as the energy of data and reference symbols, respectively [11]. In OFDM-DCSK based systems [10], considering one chaotic reference sequence is needed for transmitting information bits in other $N-1$ subcarriers, the bit energy can be denoted as $E_b = E_{data} + E_{ref}/(N-1)$ [11], where $E_{data} = E_{ref} = T_c \sum_{k=0}^{\beta-1} x_k^2$. In order to facilitate the analysis of energy efficiency, here we use the data-energy-to-bit-energy-ratio (DBR) to define the energy efficiency denoted as:

$$DBR = \frac{E_{data}}{E_b}. \tag{18}$$

Based on (18), we can obtain that the energy efficiency of the proposed system and benchmark systems. For example, the conventional OFDM-DCSK system [10] has the DBR of $(N-1)/N$, while in this research work, with the proposed PC-IM-MPSK-OFDM-DSCK scheme, the energy efficiency can be remarkably improved. Moreover, thanks to the application of the pre-distortion module at the transmitter, the number of transmitted index bits in CI codes aided OFDM-DCSK symbol can remain the same when the modulation order increases. Note that our proposed scheme can use N subcarriers to transmit $(N-1)\log_2 M$ bits via MPSK symbol and $\log_2 N$ bits via index modulated symbol, the DBR of our proposed scheme can be evaluated as $((N-1)\log_2 M + \log_2 N)/N$.

Table I compares the energy efficiency of counterpart DCSK system [6], OFDM-DCSK system [10], carrier index MC-DCSK [24], MC M-ary DCSK [21], CI aided OFDM-DCSK based system [27], the EECI aided OFDM-DCSK system [29] and our proposed PC-IM-MPSK-OFDM-DSCK system. We can conclude from the table that thanks to the parallel architecture design, the proposed scheme can reach an energy efficiency much larger than 1.

Moreover, it is noticeable that the proposed system achieves relatively higher energy efficiency than benchmarks. The reason why our proposed system has high energy efficiency is that on the one hand, similar to the MC M-ary DCSK [21] scheme, the

TABLE I
ENERGY EFFICIENCY COMPARISONS

System	Energy efficiency
DCSK [6]	$\frac{1}{2}$
OFDM-DCSK [10]	$\frac{N-1}{N}$
carrier index MC-DCSK [24]	$\frac{N-1+\log_2 N}{N+1}$
MC M-ary DCSK [21]	$\frac{N\log_2 M+\log_2 N}{2N}$
CI aided OFDM-DCSK [27]	$\frac{N-1}{N}$
EECI aided OFDM-DCSK [29]	$\frac{N-1+(\log_2 N)-1}{N}$
Proposed PC-IM-MPSK-OFDM-DSCK	$\frac{(N-1)\log_2 M+\log_2 N}{N}$

TABLE II
SPECTRAL EFFICIENCY COMPARISONS

System	Spectral efficiency
DCSK [6]	$\frac{1}{BT_s}$
OFDM-DCSK [10]	$\frac{N-1}{BT_s}$
carrier index MC-DCSK [24]	$\frac{N(N-1+\log_2 N)}{(N+1)BT_s}$
MC M-ary DCSK [21]	$\frac{N\log_2 M+\log_2 N}{2BT_s}$
CI aided OFDM-DCSK [27]	$\frac{N-1}{BT_s}$
EECI aided OFDM-DCSK [29]	$\frac{N-1+(\log_2 N)-1}{BT_s}$
Proposed PC-IM-MPSK-OFDM-DSCK	$\frac{(N-1)\log_2 M+\log_2 N}{BT_s}$

M-ary modulation increases the number of bit $\log_2 M$ times. On the other hand, the information bits carried by the CI codes will not consume additional energy, thus more bits could be delivered while the total energy remains unchanged. Namely, both the M-ary modulation and the index modulation enable the multi carrier DCSK system to deliver more bits with no requirement of additional energy. As a result, the energy efficiency could be improved.

Subsequently, we compare the spectral efficiency of the proposed system with benchmark scheme. For fairness of comparisons, we assume that all considered schemes occupy the same bandwidth of B, and the duration is T_s. Then we calculate the spectral efficiency by evaluating the number of bits transmitted per bandwidth per duration. As shown in Table II , we can observe that our proposed scheme achieves higher spectral efficiency than other benchmark schemes.

B. PAPR Performance

The PAPR performance is evaluated by calculating the complementary cumulative distribution function (CCDF) which is denoted as: [26], [27], [29]

$$CCDF(PAPR_0) = Pr(PAPR > PAPR_0), \tag{19}$$

where $Pr(A)$ denotes the probability of A and $PAPR_0$ denotes a PAPR threshold. The PAPR of samples χ_p in one OFDM-DCSK symbol duration T_s containing β OFDM symbols is denoted as $PAPR = \max(|\chi_p|^2)/\mathrm{E}\{|\chi_p|^2\}$, where $\max(\cdot)$ takes the maximum value [29].

It is worth pointing out that both the index modulation and MPSK will not increase the PAPR since their rotation operation and constant-envelop constellation mappings will not change the PAPR.

C. GA-Aided BER Analysis

We could use the Gaussian approximation (GA) method [31] to derive the approximate BER expressions or apply the numerical methods such as the series expansion to obtain the BER bound [32]. In this paper, the GA method [31] is used to derive the BER expression, which provides higher approximation precision when the number of samples is larger, e.g., larger chaotic sequence length β or larger number of subcarriers N or modulation order M.

Considering the circular rotation pattern of the CI codes matrix is limited, the number of information bits modulated by the index is small. In addition, as indicated by (16), the estimates of the index bits are obtained via calculating the argument of constellation points. Since both the index modulated symbols and the MPSK modulated symbols experience the same processing OFDM modules and channel fading, the BER performances would be close. However, since the orthogonality of the CI codes matrix helps to reduce the interference among symbols, the interference among symbols could be reduced, thereby leading to slightly better BER performances, thus slightly different reliability performances could be provided respectively by the index modulation and the MPSK modulation. Nevertheless, considering that no explicit statistical distribution could be given for the index bits due to the irregular argument of constellation points, here we mainly focus on the BER of bits modulated by the MPSK module. It is worth mentioning that the overall BER performances approach the BER performances of the index modulated and the MPSK modulated symbols close to each other, which will be demonstrated by the simulation results in the following Section.

Assuming that the duration of one chaotic chip is $T_c = 1$, the number of bits contained in the set modulated by the CI codes matrix is $N_i = \log_2 N$, the number of bits in another set modulated by MPSK is $N_{all} = \log_2 M(N-1) + N_i$. Besides, we assume that i_0 can be recovered reliably at the receiver.

Based on the above assumptions, we can derive that $E_{data} = \beta\mathrm{E}\{x_k^2\}$ and $E_b = N^2\beta\mathrm{E}\{x_k^2\}/N_{all}$. For $n \geq 1$, define $K_n = e^{-j2\pi\hat{i}_0 n/(MN)}(\sum_{i=0}^{N-1} H_i \sum_{m=0}^{N-1} s_m u_{i_0/M}^m u_i^{(m-n)})$, then the demodulated symbol $\hat{Z}_n$ can be further derived from (8) and (17) as:

$$\hat{Z}_n = \underbrace{\sum_{k=1}^{\beta} x_k \left(K_n \mathbb{R}\left\{ \sum_{i=0}^{N-1} \xi_{i,k} \right\} + \mathbb{R}\left\{K_0\right\} \sum_{i=0}^{N-1} \xi_{i,k}^{(n)} \right)}_{G_1}$$
$$+ \underbrace{\mathbb{R}\left\{K_0\right\} K_n \sum_{k=1}^{\beta} x_k^2}_{G_2} + \underbrace{\sum_{k=1}^{\beta} \mathbb{R}\left\{ \sum_{i=0}^{N-1} \xi_{i,k} \right\} \sum_{i=0}^{N-1} \xi_{i,k}^{(n)}}_{G_3}, \tag{20}$$

where G_2 denotes the desired signal, while G_1 and G_3 denote the interference components. Since G_1, G_2 and G_3 are independent;

we can further derive the expectation and variance of $\hat{Z}_n$ as [31]:

$$\mathrm{E}\{\hat{Z}_n|s_n\}=\sum_{\omega=1}^{3}\mathrm{E}\{G_\omega|s_n\},\ \mathrm{var}\{\hat{Z}_n|s_n\}=\sum_{\omega=1}^{3}\mathrm{var}\{G_\omega|s_n\}. \tag{21}$$

Based on the derived statistical characteristics given by (21), we could further derive the signal-to-noise-plus-interference ratio (SINR) expression for BER derivations as [30]:

$$\Gamma=\frac{\mathrm{E}\{Z_n|s_n\}^2}{\mathrm{var}\{Z_n|s_n\}}. \tag{22}$$

Next, with reference to the general BER expression given in [33], using the SINR expression presented above, we express the BER performance over AWGN channel as:

$$P_b=\frac{1}{\log_2 M}\sum_{c=1}^{\log_2 M}P_b(c). \tag{23}$$

where c is the index of bits in an MPSK symbol, and $1\le c\le \log_2 M$. For $c\le 3$, $P_b(c)$ can be defined as [33]:

$$P_b(c)=\sum_{m=0}^{\eta}\left\{\frac{2^{2-\lfloor 2/M\rfloor}}{M}\cdot Q\left(\sqrt{\Gamma\log_2 M}\sin\frac{(2m+1)\pi}{M}\right)\right\} \tag{24}$$

where $Q(x)=\int_x^\infty 1/\sqrt{2\pi}e^{-t^2/2}\mathrm{d}t$ is the 1-D Q-function. When $c>3$, $P_b(c)$ can be defined as [33]:

$$\begin{aligned}P_b(c)&=\sum_{m=0}^{2^{\log_2 M-2}-1}\left\{C_1(m)\cdot Q\left(\sqrt{\Gamma\log_2 M}\sin\frac{\phi_1(m)\pi}{M}\right)\right\}\\&+\sum_{l=0}^{\frac{M}{2^c}(2^{c-2}-1)-1}\left\{C_2(l)\cdot Q\Bigg(\sqrt{\Gamma\log_2 M}\sin\frac{\phi_2(l)\pi}{M},\right.\\&\left.\sqrt{\Gamma\log_2 M}\sin\frac{\phi_3(l)\pi}{M};-\rho\Bigg)\right\}\end{aligned} \tag{25}$$

where $C_1(m)=(2^c/M)(-1)^{\lfloor n\cdot 2^{c-1}/M\rfloor}$, $\phi_1(n)=2n+1$, $C_2(l)=(2^{k+1}/M)(1+\lfloor(4l/M)+(1/2^{\lfloor 2^{3-c}\rfloor+c-3})\rfloor)\cdot(-1)^{\lfloor 3/c\rfloor+\lfloor l\cdot 2^{c-1}/M}$, $\phi_2(l)=(M/2)-2l-1$, $\phi_3(l)=2^{\log_2 M-k+1}+\sum_{h=0}^{\log_2 M-c}(2^h\cdot(-1)^{\lfloor l/2^h\rfloor+1})$, $\rho=\cos((\phi_2(l)+\phi_3(l))\pi/M)$[33], and the 2-D Q-function can be defined as $Q(x_1,x_2,\rho)=1/((1/\sqrt{2\pi})\cdot(1-\rho^2))\cdot\int_{x_2}^\infty\int_{x_1}^\infty e^{-(x^2+y^2-2\rho xy)/(2\cdot(1-\rho^2))}\mathrm{d}x\mathrm{d}y$.

Furthermore, the average BER over the frequency selective fading (FSF) channel can be derived as the integration of the conditional BER of each path, which can be denoted as [30]:

$$P_{FSF}=\int_0^\infty\cdots\int_0^\infty P_b f(\Omega_1),\ldots,f(\Omega_L)\mathrm{d}\Omega_1,\ldots,\mathrm{d}\Omega_L \tag{26}$$

where $\Omega_l=|\alpha_l|^2$ is the power of each path and its probability density function (PDF) can be denoted as $f(\Omega_l)=(e^{-\Omega_l/\mathrm{E}\{\Omega_l\}})/\mathrm{E}\{\Omega_l\}$.

Then the general BER over flat fading channel can also be derived as:

$$P_{flat}=\int_0^\infty P_b f(\Omega_1)\mathrm{d}\Omega_1. \tag{27}$$

Specifically, take $M=2$ and $M=4$ as two examples, more details about the derivations are given as follows.

1) $M=2$: When $M=2$, the constellation points are denoted as $+1,-1$. The conditional BER can be calculated by the SINR as $\mathrm{erfc}(\sqrt{\Gamma/2})/2$, where $\mathrm{erfc}(x)=2\int_x^\infty e^{-t^2}\mathrm{d}t/\sqrt{\pi}$. For the flat fading channel, we have $H_i=H$ for $\forall i$. Then the statistical characteristics of G_1, G_2, and G_3 are derived as below.

$$\mathrm{E}\{G_1|(s_n=\pm1)\}=\mathrm{E}\{G_3|(s_n=\pm1)\}=0, \tag{28a}$$

$$\mathrm{E}\{G_2|(s_n=+1)\}=-\mathrm{E}\{G_2|(s_n=-1)\}=N^2|H|^2\beta\mathrm{E}\{x_k^2\}, \tag{28b}$$

$$\mathrm{var}\{G_{1r}|(s_n=\pm1)\}=N^3|H|^2\beta\mathrm{E}\{x_k^2\}N_0, \tag{28c}$$

$$\mathrm{var}\{G_{1i}|(s_n=\pm1)\}=\frac{1}{2}N^3|H|^2\beta\mathrm{E}\{x_k^2\}N_0, \tag{28d}$$

$$\mathrm{var}\{G_2|(s_n=\pm1)\}=N^4|H|^4\beta\mathrm{var}\{x_k^2\}, \tag{28e}$$

$$\mathrm{var}\{G_{3r}|(s_n=\pm1)\}=\mathrm{var}\{G_{3i}|(s_n=\pm1)\}=\frac{1}{4}N^2\beta N_0^2, \tag{28f}$$

where G_{1r} and G_{1i} denote the real and imaginary part of G_1, respectively, and the real and imaginary part of G_2, and G_3 can be defined in a similar way. Considering that when $M=2$, s_n is a real number, then the imaginary part of G_ω can be ignored.

Define $\gamma=|H|^2E_b/N_0$ and the PDF of γ as $f(\gamma)$ where $f(\gamma)=(e^{-\gamma/\mathrm{E}\{\gamma\}})/\mathrm{E}\{\gamma\}$ over the flat fading channel, thanks to the statistical characteristics of G_1, G_2 and G_3. The average BER over flat fading channel when $M=2$ can be derived according to (21), (22) and (28) as:

$$\begin{aligned}P_{2,flat}&=\int_0^\infty\frac{1}{2}\mathrm{erfc}\left(\sqrt{\frac{\Gamma}{2}}\right)f(\gamma)\mathrm{d}\gamma\\&=\int_0^\infty\frac{1}{2}\mathrm{erfc}\left(\sqrt{\frac{\mathrm{E}\{Z_n|s_n\}^2}{2\mathrm{var}\{Z_n|s_n\}}}\right)f(\gamma)\mathrm{d}\gamma\\&=\int_0^\infty\frac{1}{2}\mathrm{erfc}\left(\sqrt{\frac{\left(\sum_{\omega=1}^3\mathrm{E}\{G_\omega|s_n\}\right)^2}{2\sum_{\omega=1}^3\mathrm{var}\{G_\omega|s_n\}}}\right)f(\gamma)\mathrm{d}\gamma\\&=\int_0^\infty\frac{1}{2}\mathrm{erfc}\left[\left(\frac{2\sum_{\omega=1}^3\mathrm{var}\{G_\omega|s_n\}}{\left(\sum_{\omega=1}^3\mathrm{E}\{G_\omega|s_n\}\right)^2}\right)^{-\frac{1}{2}}\right]f(\gamma)\mathrm{d}\gamma\\&=\int_0^\infty\frac{1}{2}\mathrm{erfc}\left[\left(\frac{1}{\beta}+\frac{2}{\gamma}+\frac{\beta}{2\gamma^2}\right)^{-\frac{1}{2}}\right]f(\gamma)\mathrm{d}\gamma.\end{aligned} \tag{29}$$

For the additive white Gaussian noise (AWGN) channel, we have $H=1$ and $\gamma=E_b/N_0$ becomes a constant value. Then the integration is removed, and the BER over AWGN channel

when $M = 2$ can be calculated by:

$$P_{2,AWGN} = \frac{1}{2}\mathrm{erfc}\left[\left(\frac{1}{\beta} + \frac{2N_0}{E_b N} + \frac{N_0^2\beta}{2E_b^2 N^2}\right)^{-\frac{1}{2}}\right]. \quad (30)$$

2) $M = 4$: When $M = 4$, the constellation points can be represented as $\sqrt{2}/2 + j\sqrt{2}/2$, $-\sqrt{2}/2 - j\sqrt{2}/2$, $\sqrt{2}/2 - j\sqrt{2}/2$, $-\sqrt{2}/2 + j\sqrt{2}/2$. For the flat fading channel, the statistical characteristics of G_1, G_2 and G_3 are evaluated as follows.

$$\begin{aligned}
&\mathrm{E}\left\{G_1|\left(s_n = \pm\frac{\sqrt{2}}{2} \pm j\frac{\sqrt{2}}{2}\right)\right\} \\
&= \mathrm{E}\left\{G_3|\left(s_n = \pm\frac{\sqrt{2}}{2} \pm j\frac{\sqrt{2}}{2}\right)\right\} = 0, \quad (31a)\\
&\mathrm{E}\left\{G_{2r}|\left(s_n = \frac{\sqrt{2}}{2} \pm j\frac{\sqrt{2}}{2}\right)\right\} \\
&= \mathrm{E}\left\{G_{2i}|\left(s_n = \pm\frac{\sqrt{2}}{2} + j\frac{\sqrt{2}}{2}\right)\right\} \\
&= -\mathrm{E}\left\{G_{2r}|\left(s_n = -\frac{\sqrt{2}}{2} \pm j\frac{\sqrt{2}}{2}\right)\right\} \\
&= -\mathrm{E}\left\{G_{2i}|\left(s_n = \pm\frac{\sqrt{2}}{2} - j\frac{\sqrt{2}}{2}\right)\right\} = \frac{\sqrt{2}}{2}N^2|H|^2\beta\mathrm{E}\left\{x_k^2\right\}, \quad (31b)\\
&\mathrm{var}\left\{G_{1r}|\left(s_n = \pm\frac{\sqrt{2}}{2} \pm j\frac{\sqrt{2}}{2}\right)\right\} \\
&= \mathrm{var}\left\{G_{1i}|\left(s_n = \pm\frac{\sqrt{2}}{2} \pm j\frac{\sqrt{2}}{2}\right)\right\} = \frac{3}{4}N^3|H|^2\beta\mathrm{E}\left\{x_k^2\right\}N_0, \quad (31c)\\
&\mathrm{var}\left\{G_{2r}|\left(s_n = \pm\frac{\sqrt{2}}{2} \pm j\frac{\sqrt{2}}{2}\right)\right\} \\
&= \mathrm{var}\left\{G_{2i}|\left(s_n = \pm\frac{\sqrt{2}}{2} \pm j\frac{\sqrt{2}}{2}\right)\right\} \\
&= \frac{1}{2}N^4|H|^4\beta\mathrm{var}\left\{x_k^2\right\}, \quad (31d)\\
&\mathrm{var}\left\{G_{3r}|\left(s_n = \pm\frac{\sqrt{2}}{2} \pm j\frac{\sqrt{2}}{2}\right)\right\} \\
&= \mathrm{var}\left\{G_{3i}|\left(s_n = \pm\frac{\sqrt{2}}{2} \pm j\frac{\sqrt{2}}{2}\right)\right\} \\
&= \frac{1}{4}N^2\beta N_0^2. \quad (31e)
\end{aligned}$$

From (31) we can find that when $M = 4$, the statistical characteristics of the real and imaginary part are identical. Moreover, since the modulation of quadrature phase-shift keying (QPSK) symbols can be regarded as two separate orthogonal binary phase-shift keying (BPSK) modulation in the real axis and the imaginary axis, the BER of the proposed system when $M = 4$ can be calculated by evaluating the real part or imaginary part only. For the real part, the average BER over flat fading channel when $M = 4$ can be derived similar to (29) as:

$$P_{4,flat} = \int_0^\infty \frac{1}{2}\mathrm{erfc}\left[\left(\frac{1}{\beta} + \frac{3}{2\gamma} + \frac{\beta}{4\gamma^2}\right)^{-\frac{1}{2}}\right] f(\gamma)\mathrm{d}\gamma. \quad (32)$$

Then the BER over AWGN channel when $M = 4$ can be evaluated by:

$$P_{4,AWGN} = \frac{1}{2}\mathrm{erfc}\left[\left(\frac{1}{\beta} + \frac{3N_0}{2E_b N} + \frac{N_0^2\beta}{4E_b^2 N^2}\right)^{-\frac{1}{2}}\right]. \quad (33)$$

Note that the BER performance with $M = 4$ will be better than the BER performance with $M = 2$ owing to the larger signal to noise ratio (SNR) value of information bits while the Euclidean distances between adjacent constellation points are the same, which will be validated via simulation results provided in the following section. However, it is worth mentioning that when the modulation order M increases, the BER performances will degrade great due to the narrowed distances between adjacent symbols.

TABLE III
COMPLEXITY COMPARISONS

System	Complexity
OFDM-DCSK [10]	$O(\beta N \log_2 N)$
carrier index MC-DCSK [24]	$O(\beta(N+1)^2)$
MC M-ary DCSK [21]	$O(\beta N^2)$
CI aided OFDM-DCSK [27]	$O(\beta N^2)$
EECI aided OFDM-DCSK [29]	$O(\beta N^2)$
Proposed PC-IM-MPSK-OFDM-DSCK	$O(\beta N^2)$

D. Complexity

Table III compares the complexity of the proposed system and counterpart systems. It is noticeable that the complexity of our design is lower than that of the carrier index MC-DCSK systems and similar to the other energy efficient schemes, while the OFDM-DCSK system without any processing overheads has the lowest complexity. To be more specific, for the OFDM-DCSK system [10], the complexity is $O(\beta N \log_2 N)$, which is mainly dependent on the OFDM modulation involving the FFT, while for the carrier index MC-DCSK [24], the FFT can not be applied since the number of subcarriers is not the power of 2, thus the complexity is $O(\beta(N+1)^2)$. Besides, the FFT cannot be applied in the MC M-ary DCSK system neither, thus the complexity of MC M-ary DCSK is $O(\beta N^2)$. Moreover, for all CI codes spreading aided OFDM-DCSK systems, the computational complexity is mainly determined by the spreading operations, and the complexity is $O(\beta N^2)$.

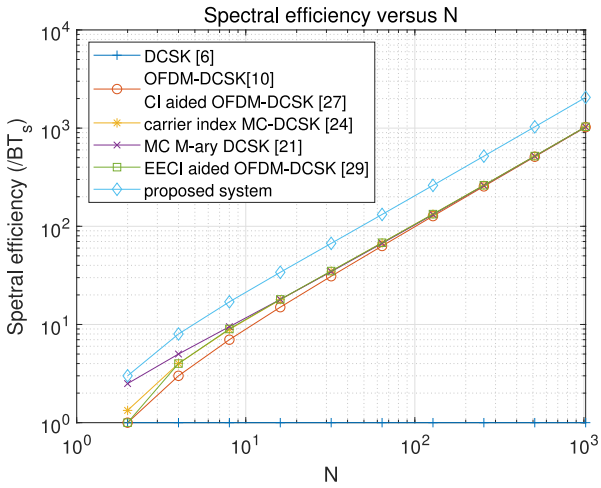

Fig. 3. Spectral efficiency performance comparison.

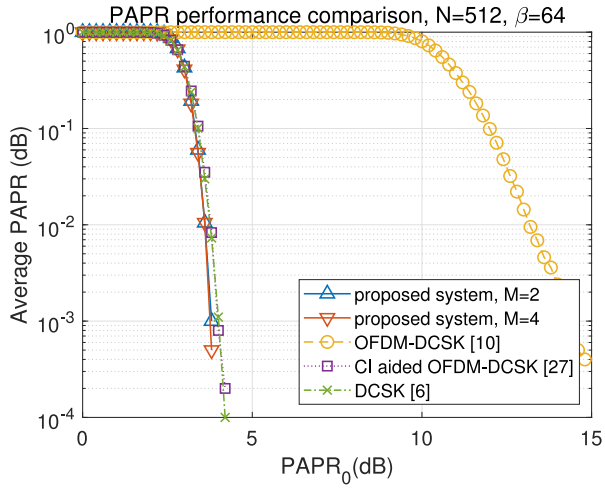

Fig. 4. PAPR performance comparison.

IV. Numerical Analysis

In this section, we will firstly present the spectral efficiency and PAPR performances, then we demonstrate the BER performances under different settings. Moreover, the performances are compared with benchmark schemes. For fairness and convenience of comparisons, the simulation parameters are set as the same as those used in the references [6], [10], [21], [24], [27], [29]. In addition, without loss of generality, with reference to [27], we also assume that perfect time and frequency synchronization could be achieved in considered systems. More details about the settings of parameters, including the number of the subcarriers, the modulation order, the length of chaotic sequences and the channel conditions etc. are presented separately in each of the following subsections.

A. Spectral Efficiency Performance

Figure 3 compares the spectral efficiency of the proposed system with those of other benchmark systems when the number of subcarriers N varies from 2 to 1000. It could be observed that the proposed system obviously has achieved better spectral efficiency than benchmark schemes no matter what the subcarrier number N is.

B. PAPR Performance

As shown in Fig. 4, the proposed parallel index modulation and MPSK aided OFDM-DCSK system have similar PAPR performances to the PAPR performance of our previous work [27] and conventional DCSK systems. In this figure, $PAPR_0$ represents the threshold, while the average PAPR refers to the average value of PAPR obtained from multiple simulations. Moreover, the PAPR performance of the proposed system is much better than the PAPR performance of conventional OFDM-DCSK [10]. The reason is that the index modulation only rotates every row of the CI codes matrix, which remains the orthogonality and the spreading CI codes [29]. We can also notice from Fig. 4 that the PAPR performance of our proposed system when $M = 4$ is equal to the PAPR performance when $M = 2$, which means that the larger value of the modulation order does not degrade the PAPR performance.

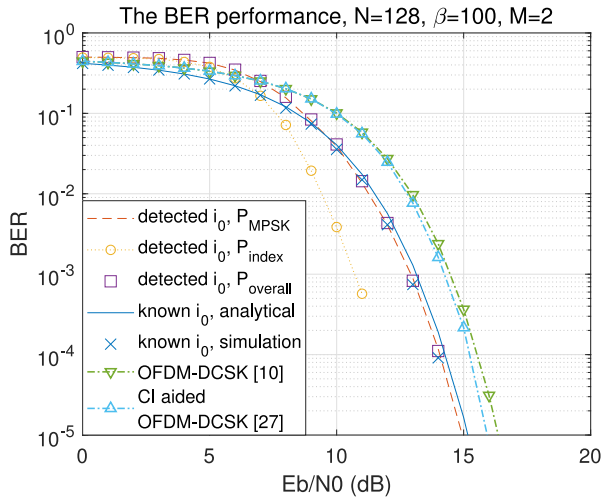

Fig. 5. The BER performance comparisons over AWGN channel.

C. BER Performance Comparisons With Benchmark Schemes

Figure 5 compares the BER performance over AWGN channel of the proposed parallel index modulation and MPSK CI aided DCSK system with the benchmark schemes when $N = 128$, $\beta = 100$, and $M = 2$. It can be observed from the figure that the proposed scheme achieves better BER performances than the benchmark OFDM-DCSK scheme [10] and the CI-aided OFDM-DCSK scheme [27], thanks to the removal of the imaginary part of the chaotic reference sequences as indicated by (10a).

In addition, we investigate the impacts of the index demodulation on the BER performance of the overall system. Let P_{MPSK}, P_{index}, and $P_{overall}$, respectively, denote the BER of MPSK modulated bits; the index modulated bits, and all information bits. We compare the BER of the proposed system in two cases that the estimate of the index $\hat{i}_0$ is obtained from the ML detection, or the exact value of i_0 is known to the receiver.

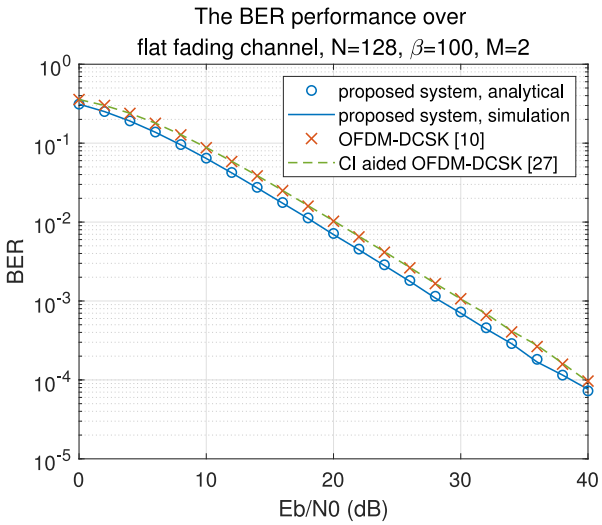

Fig. 6. The BER performances over flat fading channels.

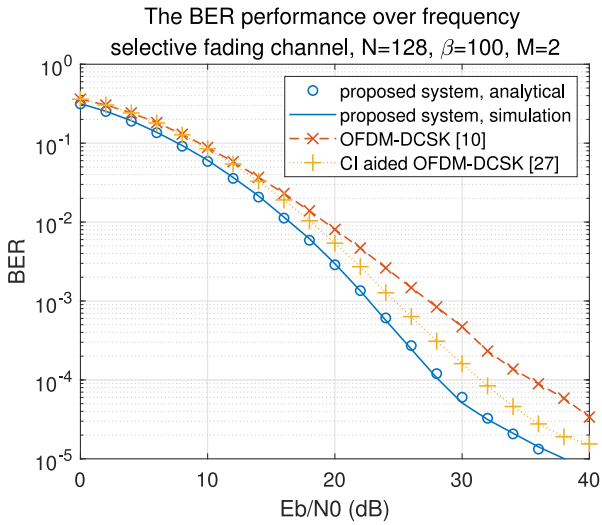

Fig. 7. The BER performances over frequency selective fading channels.

It can be seen that thanks to the orthogonality of the CI codes matrix, P_{index} is much lower than P_{MPSK} and $P_{overall}$.

Moreover, it can be observed that the estimate precision has slight influence on the overall BER, especially when SNR is relatively high. Namely, P_{MPSK} approaches $P_{overall}$, which demonstrates the claim that the overall BER can be approximated by the BER of MPSK modulated bits as mentioned in the above theoretical BER analysis. Therefore, we can apply the analytical BER expression of P_{MPSK} to evaluate the overall BER approximately.

Next, we apply the derived closed-form BER expression given by (29), and compare the theoretical analysis results with the simulated BER performances over flat fading channels when $N = 128$, $\beta = 100$, and $M = 2$ with the assumption of $\tau_{max} << 1/(N\Delta f)$. As illustrated by Fig. 6, the analytical BER performances match the simulated ones. Moreover, similar to the observations over AWGN channel, our proposed system achieves better BER performances than the conventional OFDM-DCSK system [10], and CI aided OFDM-DCSK system [27] as our proposed system only uses the real part of the chaotic reference sequences to perform the correlation demodulation, which effectively suppresses the noise or interference induced by the imaginary part.

Subsequently, Fig. 7 gives the BER performances when $N = 128$, $\beta = 100$, and $M = 2$ over the frequency selective fading (FSF) channel. The channel has three paths with the average energy of $E\{\Omega_l\} = E\{\Omega_1\}e^{-\epsilon(l-1)}$ [34], where the power decay factor is $\epsilon = 3$ and $\sum_{l=1}^{L} \Omega_l = L$. Moreover, the time delays of each path in the FSF channel can be defined as $[\tau_1, \tau_2, \tau_3] = [0, 0.05, 0.1]\mu s$ and the subcarrier spacing can be defined as 312.5 kHz [30]. It can be concluded from Fig. 7 that the analytical BER performances match the simulation results. Moreover, our proposed system achieves better BER performances than the OFDM-DCSK system [10] and CI aided OFDM-DCSK system [27] while enhancing the energy efficiency thanks to the parallel concatenated index modulation and MPSK modulation.

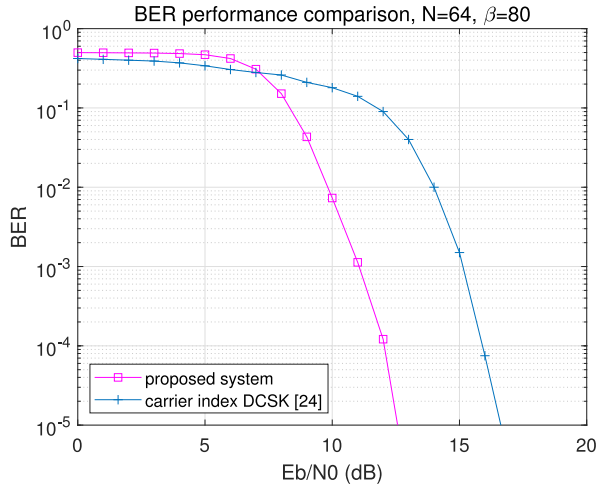

Fig. 8. BER performance comparison with carrier index DCSK [24] over AWGN channel.

Notably, comparing the results given in Fig. 6 with those in Fig. 7, we can find that the BER performances over the FSF channel are better than those over the flat fading channel. The reason is that with the aid of the CI codes spreading, larger frequency diversity gain can be achieved over the FSF channel, wherein each subcarrier might experience different channel fading, than that over the flat fading channels.

Then we select the carrier index DCSK [24] as the benchmark index based chaotic modulation scheme, which also deliver information via multiple carriers, to compare the BER performances with our design over AWGN channel. The parameters are set as $N = 64$, $\beta = 80$ and $M = 2$. It can be observed from Fig. 8 that our proposed system could achieve considerable BER performance gain when E_b/N_0 is relatively higher, while for lower E_b/N_0, the BER performances of our proposed system is slightly worse than those of the carrier index DCSK system since the orthogonality of CI codes could not be well guaranteed.

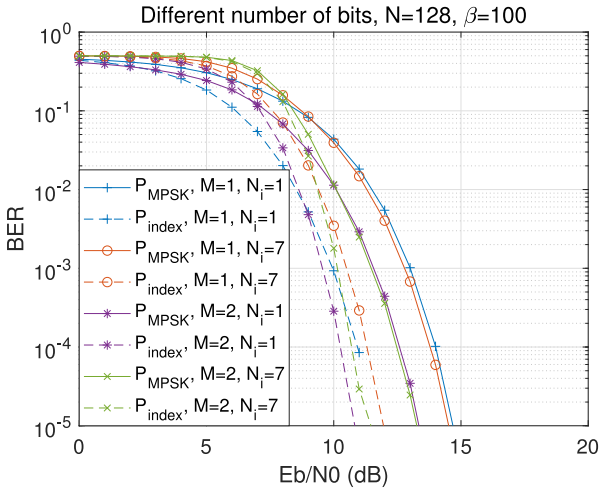

Fig. 9. BER and bit rate performance trade-offs serving different QoS demands over AWGN channel.

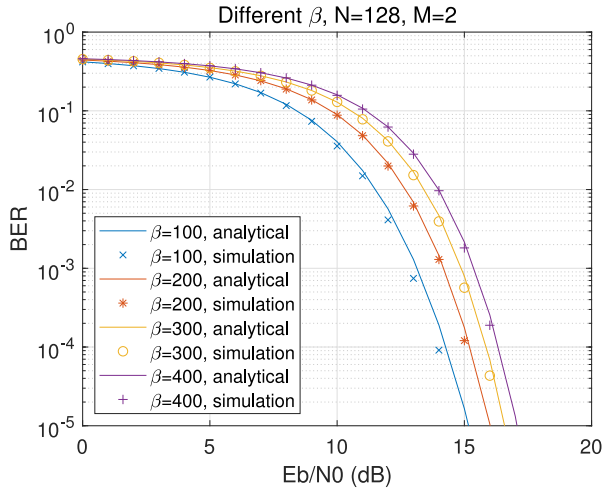

Fig. 10. The BER performances over AWGN channel when $N = 128$ and $M = 2$.

D. Data Rate and BER Trade-Offs With QoS Consideration

In this paper, as mentioned in Section I, the QoS corresponds to the data rate and the BER. In practical systems, such as IoT networks with massive connections, user terminals might have different QoS demands. For example, some user terminals might require more reliable transmissions of the data collected from the sensors, while some user terminals need high data rate transmissions to serve the real time voice delivery.

Next, inspired by the observations that the BER of index modulated bits P_{index} is lower than P_{MPSK}, in Fig. 9, we demonstrate the proposed parallel modulation scheme can provide different BER and different data rates using various combinations of the index modulation and MPSK modulations. Namely, different QoS in terms of the data rate and the BER could be provided. To be more explicit, the user data bits modulated by the M-ary modulation could be delivered with higher data rate of $(N-1)\log_2 M$ bits per slot, while the bits modulated by the indexes would be transmitted with the data rate of N_i bits per slot and lower BER of P_{index}. From Fig. 9, we can observe that when the modulation order of MPSK $M = 1, 2$ and the number of information bits $N_i = 1, 7$, the index modulated bits, and MPSK modulated bits are transmitted with different BER. It is noticeable the index modulated bits can be delivered more reliably thanks to the orthogonality of the CI code matrix. Therefore, we can use the index modulation module to transmit the key information requiring higher reliability and use the MPSK module to deliver information for users having demands of higher data rates.

E. BER Performances With Different Setting Over AWGN Channel

Then Fig. 10 shows the BER performance over the AWGN channel when $N = 128$ and $M = 2$. We can conclude that when $\beta \geq 100$, the BER performances will become worse when β increases. This is because longer chaotic sequence can collect more noise so that the noise power increases. Moreover, we can also find from Fig. 10 that the analytical BER matches the simulated BER well.

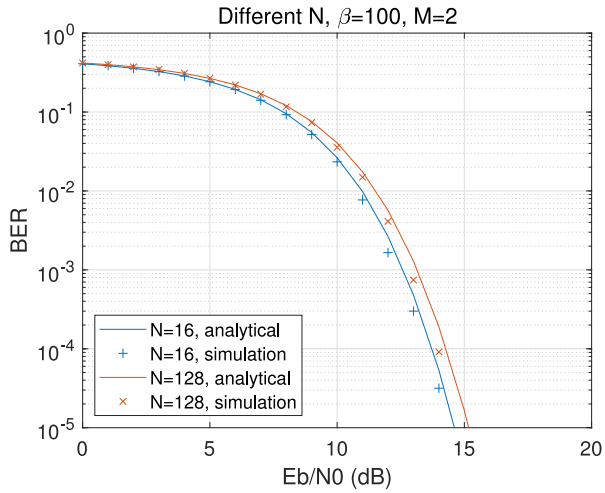

Fig. 11. The BER performances over AWGN channel when $\beta = 100$ and $M = 2$.

Figure 11 illustrates the BER performance over the AWGN channel when $\beta = 128$ and $M = 2$ in the condition of correct i_0 estimation. We can conclude from Fig. 11 that when $N \geq 16$, the BER performance will become worse when N increases. This is because of (30) we can calculate that when N is large, BER will increase with the increase of N. Moreover, we can also find from Fig. 10 that the analytical BER approach the simulated BER.

Figure 12 demonstrates the BER performance over the AWGN channel when $N = 128$ and $\beta = 100$. In Fig. 12, the BER performances when $M = 4$ are better than the BER performance when $M = 2$, which matches the conclusion jointly made by (30) and (33). Moreover, it can also seen that the analytical BER performance can also fit the simulated BER performance well.

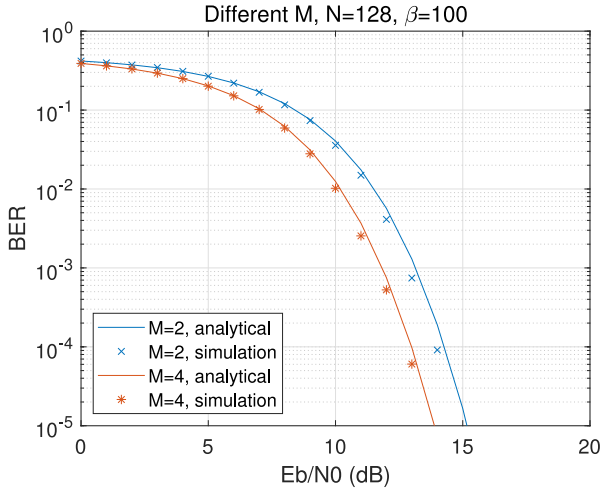

Fig. 12. The BER performances over AWGN channel when $N = 128$ and $\beta = 100$.

Last but not the least, it is worth pointing out that if higher order modulation scheme or the amplitude modulation schemes such as QAM or amplitude shift keying (ASK) are applied, due to the narrowed Euclidean distances between symbols or the increasing interference to chaotic transmissions, the BER performances would degrade accordingly.

V. Conclusion

In this paper, we propose a QoS-aware parallel concatenated index modulation and MPSK modulation aided OFDM-DCSK scheme, to simultaneously provide different QoS services, enhance the energy efficiency as well as the reliability, and suppress the PAPR. We divide the information bits into two parallel sets. One set of bits is converted to the decimal number to rotate the CI codes matrix circularly; thus the index is utilized to carry the information bits. Another set of bits are modulated by the MPSK modulation module. Then we add a pre-distortion module to avoid the phase ambiguity induced by the index modulation. Subsequently, the MPSK symbols are modulated by the chaotic reference sequence and further spread by the information-bearing CI codes matrix. After IFFT and adding CP, the user data are delivered via multiple subcarriers. At the receiver, the information bits embedded in the index and modulated by MPSK are sequentially recovered. Furthermore, we analyze the energy efficiency, spectral efficiency, PAPR, BER and complexity performances and compare them with benchmark schemes. Simulations demonstrate that our proposed scheme outperforms the benchmark schemes. With our design, various BER and different data rate can be provided by different combinations of the index modulation and the MPSK. Moreover, better energy efficiency, spectral efficiency and reliability performances can be achieved than benchmark schemes. The potential applications include IoT terminals with low power consumption requirements or millimeter-wave band communications serving massive nodes with different QoS demands.

References

[1] D. Liu *et al.*, "User association in 5G networks: A survey and an outlook," *Commun. Surveys Tuts.*, vol. 18, pp. 1018–1044, Apr.–Jun. 2016.
[2] M. Agiwal, A. Roy, and N. Saxena, "Next generation 5G wireless networks: A comprehensive survey," *Commun. Surveys Tuts.*, vol. 18, pp. 1617–1655, Jul.–Sep. 2016.
[3] F. C. M. Lau and C. K. Tse, *Chaos-Based Digital Communication Systems*. New York, NY, USA: Springer, 2003.
[4] P. Stavroulakis, *Chaos Applications in Telecommunicaitons*. Boca Raton, FL, USA: CRC Press, 2005.
[5] H. Dedieu, M. P. Kennedy, and M. Hasler, "Chaos shift keying: Modulation and demodulation of a chaotic carrier using self-sychronizing Chua's circuits," *IEEE Trans. Circuits Syst. II, Analog Digit. Signal Process.*, vol. 40, no. 10, pp. 634–642, Oct. 1993.
[6] G. Kolumbán, B. Vizvári, W. Schwarz, and A. Abel, "Differential chaos shift keying: A robust coding for chaos communication," in *Proc. NDES'96*, 1996, pp. 87–92.
[7] Z. Galias and G. M. Maggio, "Quadrature chaos-shift keying: Theory and performance analysis," *IEEE Trans. Circuits Syst. I, Fundam. Theory Appl.*, vol. 48, no. 12, pp. 1510–1519, Dec. 2001.
[8] H. Yang and G. P. Jiang, "High-efficiency differential-chaos-shift-keying scheme for chaos-based noncoherent communication," *IEEE Trans. Circuits Syst. II, Exp. Briefs*, vol. 59, no. 5, pp. 312–316, May 2012.
[9] G. Kaddoum, F. D. Richardson, and F. Gagnon, "Design and analysis of a multi-carrier differential chaos shift keying communication system," *IEEE Trans. Commun.*, vol. 61, no. 8, pp. 3281–3291, Aug. 2013.
[10] S. Li, Y. Zhao, and Z. Wu, "Design and analysis of an OFDM-based differential chaos shift keying communication system," *J. Commun.*, vol. 10, pp. 199–205, Mar. 2015.
[11] G. Kaddoum, "Design and performance analysis of a multiuser OFDM based differential chaos shift keying communication system," *IEEE Trans. Commun.*, vol. 64, no. 1, pp. 249–260, Jan. 2016.
[12] P. Chen, Y. Fang, K. Su, and G. Chen, "Design of a capacity-approaching chaos-based multiaccess transmission system," *IEEE Trans. Vehi. Tech.*, vol. 66, no. 12, pp. 10806–10816, Dec. 2017.
[13] X. Cai, W. Xu, L. Wang, and F. Xu, "M-ary code-shifted differential chaos shift keying with in-phase and quadrature code index modulation," *IET Commun.*, vol. 13, no. 19, pp. 3253–3259, 2019.
[14] G. Cai, Y. Fan, G. Han, F. C. M. Lau, and L. Wang, "A square-constellation-based M-ary DCSK communication system," *IEEE Access*, vol. 4, pp. 6295–6303, Sep. 2016.
[15] P. Chen, L. Shi, Y. Fang, G. Cai, L. Wang, and G. Chen, "A coded DCSK modulation system over rayleigh fading channels," *IEEE Trans. Commun.*, vol. 66, no. 9, pp. 3930–3942, Sep. 2018.
[16] G. Kaddoum, M. F. A. Ahmed, and Y. Nijsure, "Code index modulation: a high data rate and energy efficient communication system," *IEEE Commun. Lett.*, vol. 19, no. 2, pp. 175–178, Feb. 2015.
[17] F. Cogen, E. Aydin, N. Kabaoglu, E. Bagar, and H. Ilhan, "A novel MIMO scheme based on code-index modulation and spatial modulation," in *Proc. 26th Signal Process. Commun. Appl. Conf.*, 2018, pp. 1–4.
[18] E. Aydin, F. Cogen, and E. Basar, "Code-index modulation aided quadrature spatial modulation for high-rate MIMO systems," *IEEE Trans. Veh. Technol.*, vol. 68, no. 10, pp. 10257–10261, Oct. 2019.
[19] W. Xu, Y. Tan, F. C. M. Lau, and G. Kolumbán, "Design and optimization of differential chaos shift keying scheme with code index modulation," *IEEE Trans. Commun.*, vol. 66, no. 5, pp. 1970–1980, May 2018.
[20] Y. Tan, W. Xu, W. Hu, and L. Wang, "Efficient and robust M-ary differential chaos shift keying scheme with code index modulation," *IET Commun.*, vol. 13, no. 2, pp. 232–242, 2019.
[21] G. Cai, Y. Fang, J. Wen, S. Mumtaz, Y. Song, and V. Frascolla, "Multi-carrier M-ary DCSK system with code index modulation: An efficient solution for chaotic communications," *IEEE J. Sel. Signal Process.*, vol. 13, no. 6, pp. 1375–1386, Oct. 2019.
[22] M. Herceg, D. Vranješ, G. Kaddoum, and E. Soujeri, "Commutation code index DCSK modulation technique for high-data-rate communication systems," *IEEE Trans. Circuits Syst. II: Express Briefs*, vol. 65, no. 12, pp. 1954–1958, Dec. 2018.
[23] M. Herceg, G. Kaddoum, D. Vranješ, and E. Soujeri, "Permutation index DCSK modulation technique for secure multiuser high-data-rate communication systems," *IEEE Trans. Veh. Technol.*, vol. 67, no. 4, pp. 2997–3011, Apr. 2018.
[24] G. Cheng, L. Wang, W. Xu, and G. Chen, "Carrier index differential chaos shift keying modulation," *IEEE Trans. Circuits Syst. II: Express Briefs*, vol. 64, no. 8, pp. 907–911, Aug. 2017.

[25] Y. Fang, G. Han, P. Chen, F. C. M. Lau, G. Chen, and L. Wang, "A survey on DCSK-based communication systems and their application to UWB scenarios," *Commun. Surveys Tuts.*, vol. 18, pp. 1804–1837, Jul.–Sep. 2016.
[26] T. Huang, L. Wang, W. Xu, and F. G. Chen, "A multi-carrier M-ary differential chaos shift keying system with low PAPR," *IEEE Access*, vol. 5, pp. 18793–18803, Sep. 2017.
[27] Z. Liu, L. Zhang, and Z. Chen, "Low PAPR OFDM-based DCSK design with carrier interferometry spreading codes," *IEEE Commun. Lett.*, vol. 22, no. 8, pp. 1588–1591, Aug. 2018.
[28] Y. Rong and Y. Hua, "Space-time power scheduling of MIMO links-fairness and QoS considerations," *IEEE J. Sel. Topics Signal Process.*, vol. 2, no. 2, pp. 171–180, Apr. 2008.
[29] Z. Liu, L. Zhang, Z. Wu, and J. Bian, "Carrier interferometry code index modulation aided OFDM-based DCSK communications," in *Proc. IEEE 90th Veh. Technol. Conf. (VTC2019-Fall)*, Sep. 2019, pp. 1–5.
[30] Z. Du, J. Cheng, and N. C. Beaulieu, "Accurate error-rate performance analysis of OFDM on frequency-selective Nakagami-m fading channels," *IEEE Trans. Commun.*, vol. 54, no. 2, pp. 319–328, Feb. 2006.
[31] Y. Xia, C. K. Tse, and F. C. M. Lau, "Performance of differential chaos-shift-keying digital communication systems over a multipath fading channel with delay spread," *IEEE Trans. Circuits Syst.II: Express Briefs*, vol. 51, no. 12, pp. 680–684, Dec. 2004.
[32] M. Dawa, G. Kaddoum, and Z. Sattar, "A generalized lower bound on the bit error rate of DCSK systems over multi-path Rayleigh fading channels," *IEEE Trans. Circuits Syst. II: Express Briefs*, vol. 65, no. 3, pp. 321–325, Mar. 2018.
[33] W. Jeong, J. Lee, and D. Yoon, "New BER expression of MPSK," *IEEE Trans. Veh. Technol.*, vol. 60, no. 4, pp. 1916–1924, May 2011.
[34] M. K. Simon and M.-S. Alouini, *Digital Communication Over Fading Channels*, 2ed., Hoboken, NJ, USA: Wiley, vol. 95, 2005.

Zhaofeng Liu received the B.S. degree in communication engineering from Sun Yat-sen University, Guangzhou, China, in 2017. He is currently working toward the master's degree in electronics and communication engineering at Sun Yat-sen University, Guangzhou, China. His research interests include chaotic communication, multicarrier communication, cognitive radio and Internet of Things.

Lin Zhang (Senior Member, IEEE) received the Ph.D. degree in information and communication engineering from Sun Yat-sen University, in 2003. She joined the School of Information Science and Technology of Sun Yat-sen University in 2003 and has served as an Associate Professor from 2007. From 2008 to 2009, she was a Visiting Researcher with the Electrical and Computer Engineering Department, University of Maryland, College Park, United States. From 2016, she joined the School of Electronics and Information Technology of Sun Yat-sen University, and also cooperated with Shandong Provincial Key Lab. of Wireless Communication Technologies. Her research has been supported by National Natural Science Foundation of China and the Science and Technology Program Project of Guangdong Province. Her current research interests are in the area of signal processing and their applications to wireless communication systems.

Zhiqiang Wu (Senior Member, IEEE) received the B.S. degree from the Beijing University of Posts and Telecommunications, in 1993, the M.S. degree from Peking University in 1996, and the Ph.D. degree from Colorado State University in 2002, all in electrical engineering. He served as an Assistant Professor at the Department of Electrical and computer Engineering, West Virginia University Institute of Technology, from 2003 to 2005. He joined Wright State University in 2005 where he currently serves as a Full Professor at the Department of Electrical Engineering. Dr. Wu's research has been supported by NSF, AFRL, ONR, AFOSR, and OFRN. He has also held visiting positions at Peking University, Harbin Engineering University, Guizhou Normal University and Tibet University.

Yuan Jiang received the Ph.D. degree from Zhejiang University, in 2004 in information and communication engineering. Currently he served as a Professor at the School of Electronics and Information Technology and the Nanhai Research Center of Sun Yat-sen University. His research has been supported by the National Key Research and Development Program of China. His current research interests are in the area of signal processing and their applications to wireless communication systems.